RSC Advances

PAPER

View Article Online
View Journal | View Issue

Cite this: *RSC Adv.*, 2020, **10**, 12217

Modulation of activator distribution by phase-separation of glass for efficient and tunable upconversion luminescence

Yi Long, Jianfeng Li, Zaijin Fang* and Bai-Ou Guan*

Received 2nd March 2020
Accepted 19th March 2020

DOI: 10.1039/d0ra01991g

rsc.li/rsc-advances

Amorphous glass is a significant luminescence matrix for various applications, such as fiber lasers, lighting and 3D data storage. However, the efficiency of luminescence, especially upconversion (UC) luminescence, in glass is usually low. The UC emission of transition metal ions is hardly observed in amorphous glass. Here, a strategy is proposed to modulate the distribution of activators based on phase-separated glass for achieving high-efficiency UC luminescence. It is demonstrated that high-efficiency UC luminescence of Yb^{3+}–Yb^{3+} pairs and Mn^{2+}–Yb^{3+} dimers are observed in the amorphous glass due to the excellent confinement of phase-separated networks to activators. The UC emission intensity of the phase-separated glass is even higher than that of all-fluoride glass. Furthermore, $KZnF_3$ and KYb_3F_{10} crystals are controllably precipitated from the glass matrix regulated by phase-separated networks. This perfectly confines activators in crystal environments, greatly enhances the UC luminescence and controllably tailors the luminescence color. This glass possesses large potential for promising application in tunable fiber lasers, multicolor displays and multiphoton excitation-based 3D optical data storage. Most importantly, the modulation strategy based on phase-separated networks paves a new way for manufacturing a wide range of optical gain materials featuring efficient and wavelength-tunable luminescence.

Introduction

Luminescent materials are of fundamental importance for various applications, such as lasers, lighting, optical communication, optical data storage, and spectroscopy.[1–3] In the past decades, activator-doped luminescent materials have garnered increasing interest due to their multiple emission wavelengths and high luminescence efficiency.[4,5] In this case, the luminescent properties of activators deeply depend on the surrounding coordination environments of the material matrix.[6,7] Amorphous glass is a significant matrix for luminescence in wide wavelength ranges.[8] The open structure of glass allows high doping concentration of activators and the amorphous feature of glass offers high optical transmittance. More importantly, the easy technique and gradual softening property of glass provide significant opportunities for the fabrication of bulk samples and profiled optical devices (*e.g.*, cambered lens or optical fibers, *etc.*) those are not available by crystal materials. Additionally, the nanocrystals can also be controllably precipitated in glass matrix due to the thermodynamically metastable features, which further diversifies the functions of glass materials.[9] These features make activator doped glass an appealing matrix for optical applications in fiber lasers, lighting and 3D data storages, *etc.*[10–12] However, the luminescence efficiency of rare earth ions in glass matrix is usually lower as compared to crystal material. Especially, the upconversion (UC) luminescence efficiency in glass matrix is generally low due to the high probability of non-radiative transition of the intermediate levels caused by the high phonon energy. Moreover, the UC luminescence of transition metal ions can hardly be observed in glass at room temperature. The bottleneck in UC efficiency of glass has greatly hindered the developments of optical devices, for example, the maximum output power of fiber lasers based on UC luminescence is below 3.0 W up to now due to the low luminescence efficiency.[13]

Previously, the traditional strategy for achieving high-efficiency UC luminescence is to incorporate the activators into glass networks featuring extremely low phonon energy, for example, fluoride, chalcogenide and halide glass networks, *etc.*[14–16] However, the requirements for high luminescence efficiency and excellent stability against crystallization of glasses are always contradictory. The poor stabilities of the glasses with low phonon energy have limited their applications in high-power laser systems. Actually, UC luminescence is a two or multi-photon process. The UC luminescence efficiency is governed by the ionic distance of activators.[17] The formation of ion pairs or dimers is possible to dramatically enhance the UC luminescence.[18,19] Accordingly, the distribution of activators in

Guangdong Provincial Key Laboratory of Optical Fiber Sensing and Communications, Institute of Photonics Technology, Jinan University, Guangzhou 510632, China. E-mail: zaijin_fang@163.com; tguanbo@jnu.edu.cn

glass network is a vital factor for modulating the UC luminescence.

Here, a novel strategy based on phase-separated network was proposed to modulate the distribution of active ions for greatly enhancing UC luminescence efficiency in glass. The rare earth ions as well as transition metal ions are both expected to be confined in the fluorine-rich networks featuring low phonon energy. The distributions of active ions are modulated by the separated fluoride networks and thus regulate the UC luminescence of glass. Moreover, the phase-separated glass possesses large potential for the precipitation of functional crystals, which further enhances and tunes the UC luminescence of activators. As a proof of concept, Yb^{3+} and Mn^{2+} ions are selected as activators to demonstrate the enhancements of UC luminescence for rare earth and transition metal ions in glass. The photoluminescence properties in combination of glass structures are carefully investigated to prove the confinement effect of the glass networks to activators, the controllable precipitation of functional crystals in glass and the advantages of this new strategy as an effective means to enhance the UC luminescence of glass for achieving efficient and tunable emissions.

Experimental

In this work, the prepared glasses (PGs) with nominal composition of x SiO_2-(100 − x)/2 ZnF_2-(100 − x)/2 KF (x = 50, 60 and 70%) were chose as host glasses because these are representative and stable candidates for phase-separated network structures.[20] These samples will be referred to as 50Si-PG, 60Si-PG and 70Si-PG glass, respectively. For Mn^{2+} and Yb^{3+} ions doping, MnF_2 and YbF_3 were selected as dopant source, the corresponding concentration was set from 0.1 to 0.5 and 0.3 mol%, respectively. All the glasses were fabricated by using a melt-quenching technique. A 30 g reagent grade stoichiometric mixture of SiO_2 (99.99%), ZnF_2 (99.99%), KF (99.99%), YbF_3 (99.9999%) and MnF_2 (99.99%) was mixed thoroughly and melted in a platinum–rhodium crucible in high temperature ranging from 1400 to 1550 °C. The glass melts were poured onto a cold brass mould and pressed with another brass plate to moulding glass samples. For obtaining glass ceramic (GC) samples, the PGs were heat treated at 540 °C according to the differential scanning calorimeter (DSC) results in our previous work.[21] The all-fluoride, silicate, germanate, tellurite glasses and GC containing $NaYF_4$ crystals are also prepared according to the previous literatures.[22–26]

The amorphous state and crystal phases in the glasses were identified by X-ray diffraction (XRD) on a D8 advance X-ray diffractometer (Bruker, Switzerland) with Cu/Kα (λ = 0.1541 nm) radiation. The emission spectra were measured by using an Edinburgh FLS980 fluorescence spectrometer (Edinburgh Instruments, UK). A 450 W xenon lamp was used as the excitation sources. The upconversion (UC) emission spectra and lifetime curves of glasses were recorded using the same spectrometer. Semiconductor lasers diode (LD), operating at 980 nm, were used as the excitation sources for UC spectra. All the measurements were performed at room temperature.

Results and discussion

For demonstrating the efficient UC luminescence in glass networks, the emission spectra of 0.3Yb^{3+} doped PGs were measured and shown in Fig. 1. Excited by using a 980 nm laser diode, blue emission peaks around 480 nm are all observed in the spectra of 0.3Yb^{3+} doped PGs as shown in Fig. 1(a). The double-logarithmic plots of the excitation power dependency on the 480 nm emission intensities, presented in Fig. 1(b), reveal that the blue emissions around 480 nm in these glasses are all two-photon processes and attributed to the UC luminescence of Yb^{3+}–Yb^{3+} pairs.[27] Moreover, it is also found from Fig. 1(a) that the UC emission intensity of 70Si-PG is about 10 times higher than that of 50Si-PG and the UC emission intensity of Yb^{3+}–Yb^{3+} pairs in PG increases dramatically when the concentration of SiO_2 is increased from 50 to 70%. These results indicate that the reasonable increase of SiO_2 in the glass networks is beneficial for the UC luminescence of Yb^{3+}–Yb^{3+} pairs. By comparison to silicate glass, the 0.3Yb^{3+} doped 70Si-PG possesses much higher UC emission intensity as shown in Fig. 1(c) due to the introduction of fluoride components in glass networks. Traditionally, all-fluoride glass (ZrF_4–BaF_2–LaF_3–AlF_3–NaF) is a desired candidate for efficient UC luminescence due to the extremely low phonon energy.[23] However, the UC emission intensity of the 0.3Yb^{3+} doped all-fluoride glass is also much lower than that of 70Si-PG as shown in Fig. 1(c). Moreover, it is also found from Fig. 1(c) that the UC emission intensity of the amorphous 70Si-PG is even higher than that of 0.3Yb^{3+} doped GC containing $NaYF_4$ crystals, which is a common candidate for high-efficiency UC luminescence.[26] The amorphous state of the 70Si-PG and the crystalline phase of the GC are proved by Fig. 1(d). Despite the

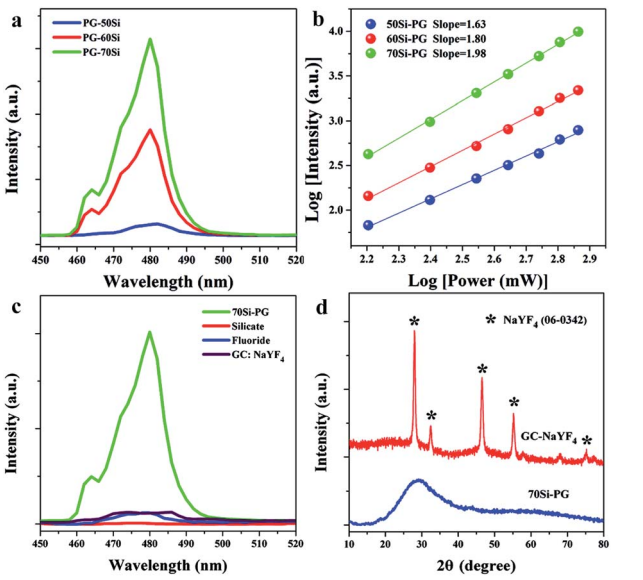

Fig. 1 (a) UC emission spectra of 0.3Yb^{3+} doped PGs containing different concentrations of SiO_2. (b) Double-logarithmic plots of the excitation power dependency on the 480 nm emission intensity of 0.3Yb^{3+} doped PGs. (c) UC emission spectra of 0.3Yb^{3+} doped 70Si-PG and other common glasses and GC. (d) XRD patterns of 0.3Yb^{3+} doped 70Si-PG and GC containing $NaYF_4$ crystals.

$0.3Yb^{3+}$ is not the optimal doping level for the all glasses, the much more intense UC emission of $0.3Yb^{3+}$ doped 70Si-PG proves it is an excellent amorphous matrix for high-efficiency UC luminescence of Yb^{3+}–Yb^{3+} pairs.

Similarly, excited by using a 980 nm laser diode, yellow broadband emissions centered at 580 nm are all observed in the three spectra of $0.3Mn^{2+}$–$0.3Yb^{3+}$ codoped PGs as shown in Fig. 2(a). All these emissions are proved to a two-photon process (Fig. 2(b)), indicating that the broadband emissions are attributed to the UC luminescence of Mn^{2+}–Yb^{3+} pairs as similar to the previous investigation.[28] In the previous investigations, the UC emissions of Mn^{2+}–Yb^{3+} pairs were usually observed in halide crystals at low temperature due to the low probabilities of non-radiative transitions. For some specific crystals, such as $MgGa_2O_4$, CaO and $GdMgB_5O_{10}$,[29–31] the UC emissions of Mn^{2+}–Yb^{3+} pairs were observed at room temperature when the activators were confined in crystal environments with short ionic distances. To the best of our knowledge, there is no report about the UC luminescence of Mn^{2+}–Yb^{3+} pairs in amorphous glass matrix. As shown in Fig. 2(c), no obvious emission band is observed in the spectra of the traditional glasses, such as silicate, germanate, fluorosilicate and tellurite glasses. Despite the all-fluoride glass possesses low phonon energy, the UC emission band of Mn^{2+}–Yb^{3+} pairs is also not observed in the spectrum as presented in Fig. 2(c). These results indicate that the UC luminescence of Mn^{2+}–Yb^{3+} pairs is not only governed by the phonon energy of matrix. The XRD pattern, shown in Fig. 2(d), reveals that no crystal has precipitated in the Mn^{2+}–Yb^{3+} coped PG. The PGs pave a new way for manufacturing amorphous optical materials featuring broadband UC luminescence and provide opportunities for the promising application in multicolor lighting and tunable fiber lasers.

It is also found from Fig. 2(a) that the UC emission intensity of Mn^{2+}–Yb^{3+} pairs increases monotonously when the concentration of SiO_2 in glass is reasonably increased from 50% to 70%. This result implies that the incorporation of SiO_2 into the glass networks is beneficial for the broadband UC luminescence of Mn^{2+}–Yb^{3+} pairs. Generally, the incorporation of SiO_2 into glass fastens the framework but weakens the UC emission due to the high phonon energy of Si–O bonds. However, in this work, the 70Si-PG possesses strong framework as well as the most efficient UC luminescence of Yb^{3+}–Yb^{3+} and Mn^{2+}–Yb^{3+} pairs, which provides a powerful solution to conquer the conventional contradiction between stability and luminescence efficiency in glass. Therefore, the network structures as well as the UC emission efficiency of the PGs can be simultaneously regulated by the concentration of SiO_2.

As proved by our previous work,[21] the ternary glasses with composition of $x\,SiO_2$-$(100-x)/2\,ZnF_2$-$(100-x)/2$ KF ($x = 50$, 60 and 70 mol%) were excellent matrices for phase-separated network structures. It was proved that the glass structures were separated to silicon-rich and fluorine-rich phases at nanoscale. The glass networks experienced from an interpenetrating phase-separation to droplet phase-separation networks when the concentration of SiO_2 increased from 50 to 70 mol%. The silicon-rich regions were mainly filled with Si and O elements and the glass framework was constructed by [SiO_4] units. While F as well as Zn elements distributed in the fluorine-rich regions and constructed the separated fluoride networks. According to ligand field theory, the Si–O networks are organized by [SiO_4] units with strong and compact structure,[32] which is difficult for the accommodation of activators possessing large ionic radius. Whereas, the F^- ions are likely aggregated around alkaline earth ions to maintain electrical neutrality and organize loose networks with 6 or more coordinated units.[33] Therefore, the fluorine-rich networks are more suitable for the accommodation of Yb^{3+} and Mn^{2+} ions and the activators in the PGs prefer to distribute in the separated fluoride networks. Comparing to interpenetrating phase-separation network, droplet phase-separation network exhibits more compact structure. The activators of 70Si-PG are confined in the separated and more compact fluoride networks, which possess extremely low phonon energy and are beneficial for the formation of ion pairs and thus greatly enhances the UC luminescence.

The fluoride and other common glasses usually contain network dispersant ions (La^{3+} or Al^{3+}) in compositions, exhibiting open and homogeneous network structures.[34] These glasses possess low confinement effects to activators when the active ions are evenly distributed in the networks. This makes against the formation of ion pair and leads to the low UC luminescence efficiency. Yb^{3+} can be confined in the crystal environments in the GC *via* the precipitation of $NaYF_4$ crystals. Nevertheless, a part of activators can incorporate into the crystal environments but a large number of active ions remain in the open glass phase due to the mismatch between Yb^{3+} and the substituted ion (Y^{3+}) in the GC. The confinement ability of the

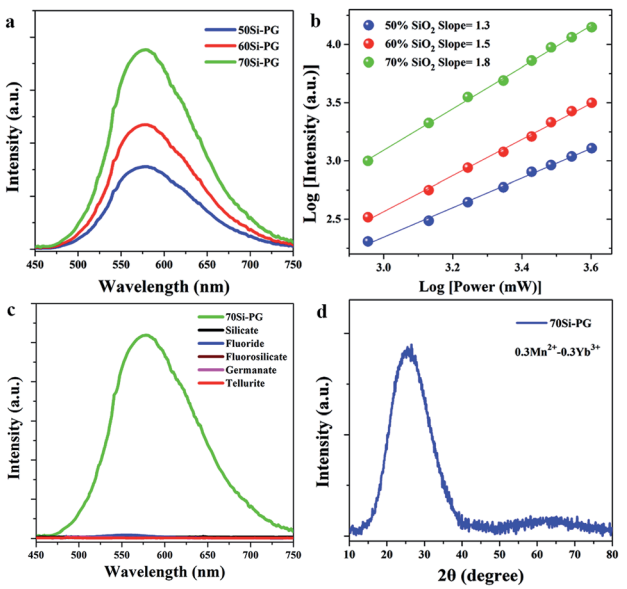

Fig. 2 (a) UC emission spectra of $0.3Yb^{3+}$–$0.3Mn^{2+}$ codoped PGs containing different concentrations of SiO_2. (b) Double-logarithmic plots of the excitation power dependency on the 580 nm emission intensity of $0.3Mn^{2+}$–$0.3Yb^{3+}$ doped glasses. (c) UC emission spectra of $0.3Yb^{3+}$–$0.3Mn^{2+}$ codoped 70Si-PG and other common glasses. (d) XRD pattern of $0.3Yb^{3+}$–$0.3Mn^{2+}$ codoped 70Si-PG.

$NaYF_4$ GC to activators is weaker than that of the phase-separated glass networks. As a result, the UC luminescence in $NaYF_4$ GC is still weaker than that in the phase-separated glass. Accordingly, we conclude that the excellent confinement of the phase-separated networks to activators in compact and low phonon energy environments are responsible for the most efficient UC luminescence of Yb^{3+}–Yb^{3+} as well as Mn^{2+}–Yb^{3+} pairs in the 70Si-GCs.

Previously, there have two explanations for the mechanism of the UC luminescence of Mn^{2+}–Yb^{3+} pairs. One is energy transfer UC mechanism. Firstly, the UC process of Yb^{3+}–Yb^{3+} pairs emits blue light. Then, the blue light is absorbed by Mn^{2+} ions and the energy is transferred to broadband emission around 580 nm.[35] The luminescence center of the energy transfer UC process is Mn^{2+} ions. The other mechanism is based on the novel luminescence centers of Mn^{2+}–Yb^{3+} dimers.[36] In some specific matrices, Mn^{2+}–Yb^{3+} dimer is formed when the ionic distance is short (~10 Å). As shown in Fig. 3(f), the ground, intermediate and excited energy levels of Mn^{2+}–Yb^{3+} dimer are presented by $|^2F_{7/2}, {}^6A_{1g}(S)\rangle$, $|^2F_{5/2}, {}^6A_{1g}(S)\rangle$ and $|^2F_{7/2}, {}^4T_{1g}(G)\rangle$, respectively. The ground state absorption of 980 nm laser contributes to the photon pumping to the intermediate level. The further excited state absorption of 980 nm photons followed by the non-radiative transition pump the electrons to the excited state. The transition of $|^2F_{7/2}, {}^4T_{1g}(G)\rangle \rightarrow |^2F_{7/2}, {}^6A_{1g}(S)\rangle$ leads to the broadband UC emission around 580 nm.

For illuminating the detailed mechanism of the UC process in these glasses, the luminescent properties of Mn^{2+}–Yb^{3+} codoped PGs are carefully investigated. Since the main UC emission peak of Yb^{3+}–Yb^{3+} pairs is located at 480 nm, the emission spectra of Mn^{2+} in the PGs were measured under the excitation of 480 nm light to compare with the UC emission spectra excited by a 980 nm laser diode. As shown in Fig. 3(a), excited by 480 nm light, the broadband emissions of Mn^{2+} ions centered at 610 nm are observed in the spectra of PGs, which are different from the UC emission spectra presented in Fig. 2(a). Moreover, the lifetime monitored at 610 nm emission and excited by 480 nm light, shown in Fig. 3(b), is 8.7, 6.9 and 6.3 ms in 50, 60 and 70Si-PGs, respectively. Whereas, the lifetime monitored at 580 nm emission and excited by 980 nm laser, as shown in Fig. 3(c), is 1.1, 1.2 and 1.6 ms in 50, 60 and 70Si-PGs, respectively. The emission lifetime of Mn^{2+} is much longer than that of Mn^{2+}–Yb^{3+} pairs indicates that the UC emissions around 580 nm in PGs are not excited by 480 nm light transferred from Yb^{3+}–Yb^{3+} pairs. Furthermore, the emission intensity increases monotonously when Mn^{2+} concentration is increased from 0.1 to 0.5% excited by 480 nm light as presented in Fig. 3(d). However, the UC emission intensity, shown in Fig. 3(e), increases first and reaches a maximum at 0.3% Mn^{2+}, then decreases when the concentration of Mn^{2+} is further increased to 0.5%. This difference in emission intensity dependency on the Mn^{2+} concentration also indicates that the luminescence centers of the UC emission and the Stokes emission excited by 480 nm light are different. The broadband UC luminesce around 580 nm in the PGs is not an energy transfer UC process but attributed to the UC luminescence of Mn^{2+}–Yb^{3+} dimers as demonstrated in Fig. 3(f).

Furthermore, the UC luminescent properties of the 0.3Mn^{2+}–0.3Yb^{3+} codoped GCs based on the phase-separated glasses were measured and shown in Fig. 4(a)–(d). The UC emission of Yb^{3+}–Yb^{3+} pairs is not observed in the spectra of Mn^{2+}–Yb^{3+} codoped PGs. However, the UC emissions of Yb^{3+}–Yb^{3+} pairs around 480 nm are observed in the spectra of GCs. The slight emission peaks of Yb^{3+}–Yb^{3+} pairs are observed in the spectra of 0.3Mn^{2+}–0.3Yb^{3+} codoped 50Si-GCs as shown in Fig. 4(a). Whereas, the emission of Mn^{2+}–Yb^{3+} dimers around 580 nm in 50Si samples enhances greatly by the heat treatments and the

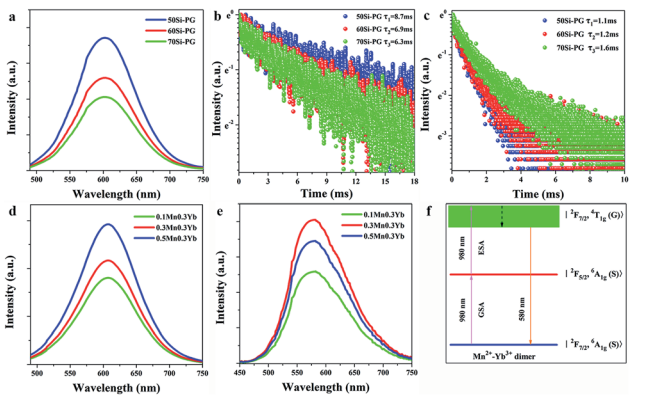

Fig. 3 (a) Emission spectra of 0.3Yb^{3+}–0.3Mn^{2+} codoped PGs excited by 480 nm light. Emission decay curves of 0.3Yb^{3+}–0.3Mn^{2+} codoped PGs excited by (b) 480 nm light and (c) 980 nm laser diode. Emission spectra of xMn^{2+}–0.3Yb^{3+} codoped PGs excited by (d) 480 nm light and (e) a 980 nm laser diode (x = 0.1, 0.3 and 0.5). (f) Energy level schematic diagram of Mn^{2+}–Yb^{3+} dimer and the related level transitions.

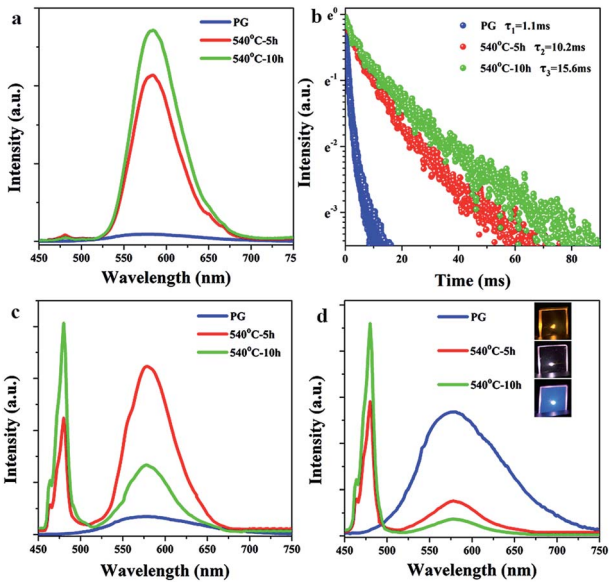

Fig. 4 (a) UC emission spectra and (b) UC emission decay curves monitored at 580 nm of 50Si-PG and GCs. UC emission spectra of (c) 60Si and (d) 70Si-PGs and GCs, the inset in (d) is the photos of samples irradiated by 980 nm laser diode.

intensity at 580 nm increases about 30 times when the sample was heat treated at 540 °C for 10 hours. Moreover, as shown in Fig. 4(b), the lifetime of the UC emission of Mn^{2+}–Yb^{3+} dimers in 50Si GCs increases from 1.1 to 10.2 and 15.6 ms when the glass was heat treated for 5 and 10 h, respectively. For 60Si-GCs, the UC emission of Yb^{3+}–Yb^{3+} pairs are observed obviously and the emission intensities at 480 nm are much higher as compared to PG. Meanwhile, the UC emission intensity of Mn^{2+}–Yb^{3+} dimers increases first under the heat treatment for 5 hours, then the emission at 580 nm decreases as the heat treatment time prolongs to 10 hours (Fig. 4(c)). For 70Si samples, the emission intensity at 580 nm decreases while the emission intensity at 480 nm increases monotonously by the heat treatments at 540 °C (Fig. 4(d)). The emission color of 70Si sample turns from yellow to white and blue after the heat treatments as shown in the inset of Fig. 4(d). These results indicate that the UC emission intensities are enhanced and the luminescence colors of the samples are tunable *via* the heat treatments.

For revealing the enhanced and tunable mechanisms of the UC luminescence, the XRD patterns of 0.3Mn^{2+}–0.3Yb^{3+} codoped GCs heat treated at 540 °C for 10 hours are shown in Fig. 5. It is found that the diffraction peaks at 31.1, 44.7, 55.5 and 64.8° are observed in the XRD patterns, which match well with the JCPDS cards of $KZnF_3$ crystal (no. 89-4110), suggesting that $KZnF_3$ crystal has precipitated in GC samples under the heat treatment. Moreover, the diffraction peaks of KYb_3F_{10} crystals (no. 74-2204) at 27.1, 31.4, 44.9 and 53.1° are also observed in the XRD patterns, proving the precipitation of KYb_3F_{10} crystals in GCs. Interestingly, it is also found from the XRD patterns that $KZnF_3$ crystals prefer to precipitate in low-silicon glass, whereas, more KYb_3F_{10} crystals are precipitated in high-silicon glass. Thus, the crystallization of the glass is regulated by the SiO_2 concentration. According to the molecular dynamics simulations reported in our previous work,[37] the PGs exhibit different phase-separated structures. For low-silicon sample, more ZnF_2 and KF are introduced into glass and distributed in the fluorine-rich regions, which leads to the low viscosity of local networks and low crystallization barrier for $KZnF_3$ crystals. More $KZnF_3$ crystals are precipitated in the 50Si-GC. For high-silicon sample, the glass networks exhibit high viscosity, $KZnF_3$ crystals are more difficult to precipitate. Yb^{3+}, possessing large ionic radius and large potential, is a nucleating agent and center for crystallization. In the 70Si-PG, Yb^{3+} ions are confined in separated fluoride networks with more compact structures and the ionic distance of Yb^{3+} ions is shorter as compared to 50Si-PG. As a result, KYb_3F_{10} crystals are easier to precipitate around Yb^{3+} in 70Si-PG due to the induced effect of nucleating agent under the heat treatments. Accordingly, the crystallizations of PGs are really regulated by the phase-separated glass networks.

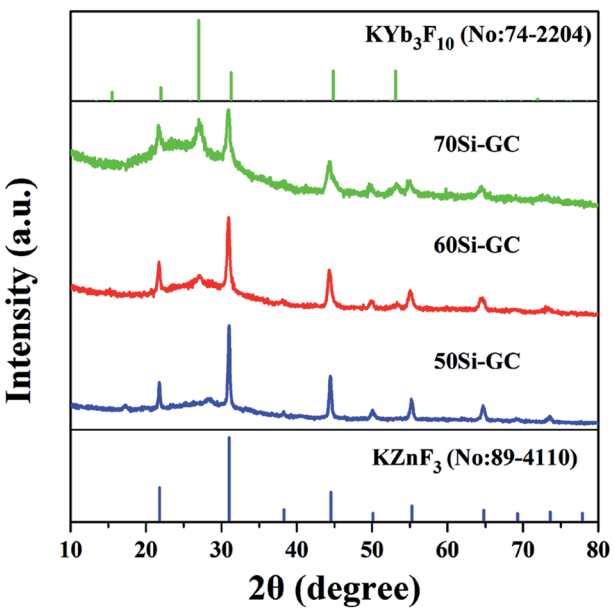

Fig. 5 XRD patterns of 0.3Yb^{3+}–0.3Mn^{2+} codoped GCs heat treated at 540 °C for 10 h and standard JCPDF cards of no. 89-4110 $KZnF_3$ and 74-2204 KYb_3F_{10} crystals.

$KZnF_3$ crystal belongs to a typical cubic perovskite structure with a $Pm\bar{3}m$ space group. This structure consists of a corner-sharing ZnF_6 octahedral 3D network, in which the Zn^{2+} ions are located at the center of the octahedron.[38] Mn^{2+} exhibits high octahedral site preference energy, similar ionic radius (R: Zn^{2+} = 0.074 nm, R: Mn^{2+} = 0.067 nm) and the same valence to Zn^{2+}, it will be likely to enter $KZnF_3$ crystals by substitution for Zn^{2+}. Besides, a small number of Yb^{3+} can enter the structure of $KZnF_3$ crystals by the substitution of K^+ as reported by E. Song.[39] The enhancements of UC emission intensity and lifetime of Mn^{2+}–Yb^{3+} dimers in 50Si-GCs (Fig. 4(a) and (b)) are ascribed to the incorporation of Mn^{2+} and Yb^{3+} into a large number of $KZnF_3$ crystals featuring lower phonon energy.

For the 60Si-GCs, a certain amount of $KZnF_3$ and KYb_3F_{10} crystals are both precipitated in the glass under the heat treatment for 5 hour. The UC emission around 480 nm is enhanced as compared to PG when Yb^{3+} ions are confined in KYb_3F_{10} crystals and Yb^{3+}–Yb^{3+} pairs are formed in crystal structures. The UC emission around 580 nm is also enhanced because of the incorporation of activators into $KZnF_3$ crystals. By the further heat treatment to 10 hours, more KYb_3F_{10} crystals are precipitated from the glass matrix, more Yb^{3+} ions enter KYb_3F_{10} crystals and deviate from Mn^{2+} ions, leading to the further formation of Yb^{3+}–Yb^{3+} pairs and the dissolution of Mn^{2+}–Yb^{3+} dimers. As a result, the UC emission of Yb^{3+}–Yb^{3+} pairs around 480 nm is further enhanced while the emission of Mn^{2+}–Yb^{3+} dimers around 580 nm is weakened. For the 70Si-GCs, a small number of $KZnF_3$ crystals but a large number of KYb_3F_{10} crystals are precipitated from glass matrix, leading to the dramatically decrease of Mn^{2+}–Yb^{3+} emission but the monotonously increase of Yb^{3+}–Yb^{3+} emission under the heat treatments. Therefore, the crystallization governed by the phase-separated networks in the glasses controllably regulates the distribution of activators and tunes the UC luminescence color of sample in wide wavelength ranges. The tunable UC luminescence in GCs depended on the selective confinement of activator in different crystals provides promising development

for the application in 3D optical data storage and 3D laser display.

Conclusions

In this work, phase-separated glasses were designed to regulate the distribution of activators and modulate the UC luminescence. It was shown that the UC luminescence intensity of Yb^{3+}–Yb^{3+} pairs in the phase-separated glass was much higher than in all-fluoride glass and even higher than in GC containing $NaYF_4$ crystals. Moreover, efficient broadband UC luminescence of Mn^{2+}–Yb^{3+} dimers was also observed in the amorphous glass at room temperature, which was not achieved in other common glasses. Furthermore, $KZnF_3$ and KYb_3F_{10} nanocrystals were controllably precipitated from the glass and regulated by the phase-separated networks. Yb^{3+} and Mn^{2+} ions were proved to be selectively confined in different crystals in the glass and thus the UC luminescence color was tuned from yellow to white and blue. This glass provides significant opportunities for the confinement of activators in compact and low phonon energy environments, which are beneficial for the formation of ion pairs or dimers and thus for achieving high-efficiency UC luminescence of rare earth ions as well as transition metal ions. The strategy based on the phase-separated glass networks paves a new way to fabricate optical gain materials for the applications in UC fiber lasers, multicolor lighting and fine optical information storages.

Conflicts of interest

There are no conflicts to declare.

Acknowledgements

The authors gratefully acknowledge the financial support from the National Natural Science Foundation of China (No. 61905093). This work was also supported by the Open Fund of the Guangdong Provincial Key Laboratory of Fiber Laser Materials and Applied Techniques (South China University of Technology) and the Fundamental Research Funds for the Central Universities (21619340).

References

1 F. Wang, Y. Han, C. S. Lim, Y. Lu, J. Wang, J. Xu, H. Chen, C. Zhang, M. Hong and X. Liu, *Nature*, 2010, **463**, 1061.
2 X. Xu, W. Zhang, D. Yang, W. Lu, J. Qiu and S. F. Yu, *Adv. Mater.*, 2016, **28**, 8045.
3 A. Fernandez-Bravol, K. Yao, E. S. Barnard, N. J. Borysl, E. S. Levy, B. Tian, C. A. Tajon, L. Moretti, M. Altoe, S. Aloni, K. Beketayev, F. Scotognella, B. E. Cohen, E. M. Chan and P. J. Schuck, *Nat. Nanotechnol.*, 2018, **13**, 572.
4 X. Liu and J. Qiu, *Chem. Soc. Rev.*, 2015, **44**, 8714.
5 X. Chen, L. Jin, W. Kong and F. Wang, *Nat. Commun.*, 2016, **7**, 10304.
6 B. Zhou, B. Shi, D. Jin and X. Liu, *Nat. Nanotechnol.*, 2015, **10**, 924.
7 J. Zhou, S. Wen, J. Liao, C. Clarke, S. A. Tawfik, W. Ren, C. Mi, F. Wang and D. Jin, *Nat. Photonics*, 2018, **12**, 154.
8 Y. Yu, Z. Fang, C. Ma, H. Inoue, G. Yang, S. Zheng, D. Chen, Z. Yang, A. Masuno, J. Orava, S. Zhou and J. Qiu, *NPG Asia Mater.*, 2016, **8**, e318.
9 S. Zhou, C. Li, G. Yang, G. Bi, B. Xu, Z. Hong, K. Miura, K. Hirao and J. Qiu, *Adv. Funct. Mater.*, 2013, **23**, 5436.
10 T. D. Bennett, J. Tan, Y. Yue, E. Baxter, C. Ducati, N. J. Terrill, H. H. M. Yeung, Z. Zhou, W. Chen, S. Henke, A. K. Cheetham and G. N. Greaves, *Nat. Commun.*, 2015, **6**, 8079.
11 B. J. Eggleton, B. Luther-Davies and K. Richardson, *Nat. Photonics*, 2011, **5**, 141.
12 M. E. Fermann and I. Hartl, *Nat. Photonics*, 2013, **7**, 868.
13 X. Zhu and N. Peyghambarian, *Adv. OptoElectron.*, 2010, **2010**, 501956.
14 W. Zhang, F. Ding and S. Y. Chou, *Adv. Mater.*, 2012, **24**, 236.
15 Q. Zhang, R. Su, X. Liu, J. Xing, T. C. Sum and Q. Xiong, *Adv. Funct. Mater.*, 2016, **26**, 6238.
16 J. J. Adams, C. Bibeau, R. H. Page, D. M. Krol, L. H. Furu and S. A. Payne, *Opt. Lett.*, 1999, **24**, 1720.
17 G. Chen, H. Qiu, P. N. Prasad and X. Chen, *Chem. Rev.*, 2014, **114**, 5161.
18 J. Wang, R. Deng, M. MacDonald, B. Chen, J. Yuan, F. Wang, D. Chi, T. Hor, P. Zhang, G. Liu, Y. Han and X. Liu, *Nat. Mater.*, 2014, **13**, 157.
19 Q. Zou, P. Huang, W. Zheng, W. You, R. Li, D. Tu, J. Xu and X. Chen, *Nanoscale*, 2017, **9**, 6521.
20 C. Lin, L. Li, S. Dai, C. Liu, Z. Zhao, C. Bocker and C. Rüssel, *J. Phys. Chem. C*, 2016, **120**, 4556.
21 Z. Fang, Z. Chen, W. Peng, C. Shao, S. Zheng, L. Hu, J. Qiu and B. Guan, *Adv. Opt. Mater.*, 2019, **7**, 1801572.
22 Z. Luo, Q. Ruan, M. Zhong, Y. Cheng, R. Yang, B. Xu, H. Xu and Z. Cai, *Opt. Lett.*, 2016, **41**, 2258.
23 E. O. Serqueira, N. O. Dantas, V. Anjos and M. J. V. Bell, *J. Alloys Compd.*, 2014, **582**, 730.
24 V. Sigaev, P. Sarkisov, P. Pernice, A. Aronne, A. Datsenko, S. Stefanovich, V. Fertikov, O. Pozhogin and D. Zakharkin, *J. Eur. Ceram. Soc.*, 2004, **24**, 1063.
25 K. Li, G. Wang, J. Zhang and L. Hu, *Solid State Commun.*, 2010, **150**, 1915.
26 F. Liu, E. Ma, D. Chen, Y. Yu and Y. Wang, *J. Phys. Chem. B*, 2006, **110**, 20843.
27 W. Qin, Z. Liu, C. Sin, C. Wu, G. Qin, Z. Chen and K. Zheng, *Light: Sci. Appl.*, 2014, **3**, e193.
28 R. Martín-Rodríguez, R. Valiente and M. Bettinelli, *Appl. Phys. Lett.*, 2009, **95**, 091913.
29 E. Song, J. Wang, D. Yu, S. Ye and Q. Zhang, *J. Mater. Chem. C*, 2014, **2**, 8811.
30 J. Wang, E. Song, M. Wu, W. Dai, X. Jiang, B. Zhou and Q. Zhang, *J. Mater. Chem. C*, 2016, **4**, 10154.
31 R. Martín-Rodríguez, R. Valiente, F. Rodríguez, F. Piccinelli, A. Speghini and M. Bettinelli, *Phys. Rev. B: Condens. Matter Mater. Phys.*, 2010, **82**, 075117.
32 S. Zhou, Q. Guo, H. Inoue, Q. Ye, A. Masuno, B. Zheng, Y. Yu and J. Qiu, *Adv. Mater.*, 2014, **26**, 7966.
33 O. Henderson-Sapir, J. Munch and D. J. Ottaway, *Opt. Express*, 2016, **27**, 6869.

34 J. Zhao, R. Ma, X. Qiao, X. Chen, B. Kang, J. Du, X. Fan, U. Ross, C. Roiland, A. Lotnyk, L. Kienle and X. Zhang, *J. Phys. Chem. C*, 2016, **120**, 17726.
35 S. Ye, Y. Li, D. Yu, G. Dong and Q. Zhang, *J. Mater. Chem.*, 2011, **21**, 3735.
36 R. Valiente, O. Wenger and H. U. Güdel, *Chem. Phys. Lett.*, 2000, **320**, 639.
37 Z. Fang, R. Cao, F. Zhang, Z. Ma, G. Dong and J. Qiu, *J. Mater. Chem. C*, 2014, **2**, 2204.
38 C. Lin, C. Liu, Z. Zhao, L. Li, C. Bocker and C. Rüssel, *Opt. Lett.*, 2015, **40**, 5263.
39 E. Song, S. Ding, M. Wu, S. Ye, F. Xiao, S. Zhou and Q. Zhang, *Adv. Opt. Mater.*, 2014, **2**, 670.